Applications of magnetooptical waveguides in integrated optics

H. Dötsch, N. Bahlmann[1], O. Zhuromskyy, M. Hammer[2], L. Wilkens, R. Gerhardt[3], P. Hertel

University of Osnabrück, D–49069 Osnabrück, Germany

A. Popkov

Zelenograd Research Institute of Physical Problems, 124360 Moscow, Russia

Abstract

Magnetooptical garnets combine high Faraday rotation with low optical losses in the near infrared region where optical communication via glass fiber is established. In this spectral range garnets are the only materials discussed to realize nonreciprocal devices as optical isolators and circulators. Although such devices are available as microoptical components, practical versions of their integrated counterparts are still lacking. Numerous concepts have been developed theoretically many of which are tested experimentally. This paper presents an overview of the state of the art of the applications of garnet films in integrated optics. Also the technique of combining garnets with semiconductor materials is shortly discussed.

1 Introduction

Optical communication via glass fiber is an attractive technique for high data rate transmission. Over the last few decades this technique was developed in the near infrared spectral region around 1.55 μm wavelength, where the optical damping of the glass fiber is minimum. The residual damping is as low as 0.2 dB per km. It is caused by Rayleigh scattering and thus cannot be avoided.

Semiconductor lasers are available as reliable light sources. It is essential that the lasers are protected from reflected light, otherwise they become unstable. For this purpose optical isolators are needed which rely on the nonreciprocal Faraday rotation of magnetooptical materials. Furthermore, for splitting and combining different transmission routes or different wavelength multiplexed signals, optical

[1]Now at Wilhelm Karmann GmbH, Osnabrück, Germany
[2]Now at University of Twente, Enschede, The Netherlands
[3]Now at DuPont, Boston, USA

circulators are required. Such nonreciprocal devices are commercially available as microoptical components.

However, to establish a wide spread affordable technique, an integration of optical devices is necessary, as occurred in the well known case of electronics. Thus, it is essential to integrate optical components like lasers, isolators, circulators, modulators, combiners, splitters, couplers etc. on a single substrate. Light is guided in such optical circuits by monomode dielectric waveguides which have lateral dimensions in the range of micrometers. As many devices rely on interference effects, the geometrical tolerances of the waveguides are very crucial.

A severe integration problem arises if materials with large refractive index differences must be combined, like semiconductors (laser–material) and garnets. Several methods have been tested to solve this problem. Furthermore, optically pumped lasers can be prepared in garnet waveguides alleviating its integration with isolators.

Although magnetic garnets must inevitably be used for nonreciprocal devices, these materials can also be applied to fabricate modulators using dynamic TE–TM mode conversion induced by high frequency excitations in the GHz–range. Applying magnetostatic volume waves, this technique has been demonstrated by Fisher et al.[1], Tamada et al.[2], Talisa[3] and by Tsai and Young[4]. Magnetostatic surface waves were used by Tsai and Young[5]. The ferrimagnetic resonance and domain resonances have been applied by Neite et al.[6] and by Winkler et al.[7], respectively. State of the art modulation techniques, however, use direct laser modulation, electroabsorption modulation or electrooptical, acustooptical and magnetooptical effects. Modulation frequencies of more than 15 GHz are reported[8].

The main purpose of this paper is to present an overview of the application of magnetooptical waveguides to realize integrated nonreciprocal devices like isolators and circulators. Finally, waveguide lasers and integration techniques, combining semiconductor and magnetooptic materials, are shortly discussed.

2 Garnet crystals

The basis for all nonreciprocal effects is the Faraday rotation. In the near infrared region, where optical glass fiber transmission is developed, magnetic garnet crystals are the only materials discussed for the realization of nonreciprocal devices, because they combine high Faraday rotation with low optical losses.

Magnetic garnets are cubic crystals having 160 ions per cubic unit cell. The chemical formula of garnets is $\{c^{3+}\}_3\ [a^{3+}]_2\ (d^{3+})_3\ O_{12}$. That means, there are three different lattice sites for the cations with respect to the surrounding oxygen anions.

The dodecahedral sites $\{c\}$ are occupied by rare earth cations and/or by Y^{3+}, La^{3+} and Bi^{3+}. The octahedral $[a]$ and tetrahedral (d) sites are ocupied by iron. The $[a]$ and (d) sublattices are coupled antiferromagnetically. As they are not equivalent, this coupling yields a ferrimagnetic crystal. The temperature dependend saturation magnetization M_s of the crystal is given by the vectorial sum of the sublattice magnetizations. Assuming that the dodecahedral lattice is not occupied by magnetically ordered paramagnetic ions, one obtains

$$M_s(T) = M_d(T) - M_a(T)\,, \tag{1}$$

where M_d and M_a denote the saturation magnetizations of the tetrahedral and octahedral sublattices, respectively.

Without substitution of Fe^{3+} by diamagnetic ions like Ga^{3+} and Al^{3+} the magnetization of the (d) sublattice dominates. Ga^{3+} and Al^{3+} are mainly incorporated on tetrahedral sites so that an increasing substitution level of these ions will lead to the dominance of the octahedral sublattice. At a certain substitution level, both sublattices are equivalent. In this case the sublattice magnetizations compensate each other and the crystal becomes antiferromagnetic. Using proper preparation techniques such a compensation can be created along a plane inside the crystal, a so called compensation wall[9].

Magnetic garnets can be grown as bulk crystals. Furthermore, high quality thin films on appropriate substrates can be obtained by epitaxial methods, like liquid phase epitaxy (LPE)[10], sputter epitaxy (SE)[11] and pulsed laser deposition (PLD)[12]. The chemical composition and the growth conditions allow to optimize the material properties for different applications. As substrate crystals gadolinium gallium garnet (GGG) or calcium–magnesium–zirconium–substituted gadolinium gallium garnet (GGCMZ) is used.

The Faraday rotation of garnets depends on the temperature T, the optical wavelength λ and on the sublattice magnetizations. These dependencies can be separated as

$$\Theta_{F,sat}(\lambda, T) = D(\lambda)\ M_d(T) + A(\lambda)\ M_a(T)\,, \tag{2}$$

where $\Theta_{F,sat}$ denotes the specific Faraday rotation per unit length if the magnetization is saturated parallel to light propagation. A and D are coefficients which only depend on the wavelength λ.

The Faraday rotation of magnetic garnets is strongly enhanced by the substitution of bismuth into the dodecahedral lattice sites of the crystals. As Bi^{3+} is a large ion, substrates with large lattice constants must be used to increase the bismuth content. Bismuth concentrations up to 2 formula units can be achieved by LPE, using gadolinium gallium garnet substrates which are substituted by the large ions of calcium, magnesium and zirconium[13]. SE and PLD allow to obtain the full bismuth concentration of 3 formula units, however on the cost of the film quality.

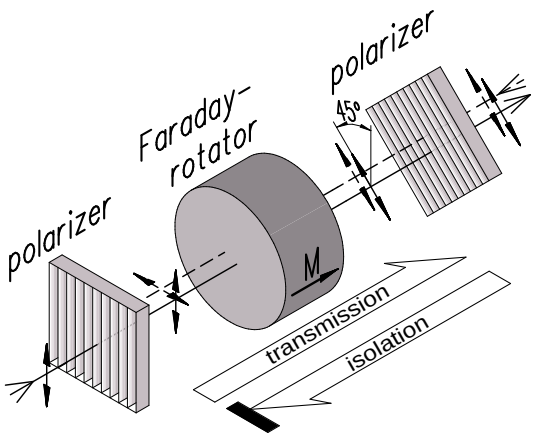

Figure 1: *Bulk optical islator, schematically.*

An even much higher Faraday rotation is possible, if cerium is substituted into the garnet crystals instead of bismuth[14]. Although cerium causes high optical losses, the quality factor, Faraday rotation per damping, is still better than for the bismuth substituted films. However, such films cannot be prepared by LPE, only by SE and PLD.

3 Optical isolators

The principle of a bulk optical isolator is sketched in Fig. 1. Incoming light is linearly polarized by the first polarizer. The plane of polarization is rotated at 45° by the Faraday rotator. Then the light passes the second polarizer, set at 45° with respect to the first one. The plane of polarization of reflected light traversing the Faraday rotator in backward direction is rotated by another 45° and thus the reflected light is blocked by the first polarizer. For practical applications, isolation of at least 30 dB and forward losses below 0.5 dB are desired. Such bulk isolators are invariant with respect to the rotation of the input polarization plane about the propagation direction, contrary to waveguide isolators discussed below.

Fig. 2 shows a monomode rib waveguide which is typically used in integrated optics. Light propagates in z–direction as quasi TM_0 or TE_0 modes which are mainly polarized along the x– and y–axis, respectively. These modes generally propagate at different propagation constants β_{TM} and β_{TE}.

Waveguide optical isolators have been intensively investigated for many years. Numerous concepts were developed and studied theoretically and experimentally, where different kinds of nonreciprocal effects are exploited. The following section gives a brief overview over these effects and over the numerical means for their modeling. Concepts of actual integrated optical isolators and circulator devices are

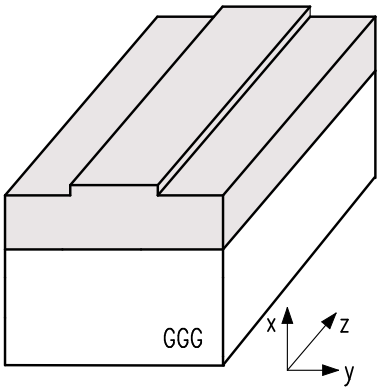

Figure 2: *Simple rib waveguide typically used in integrated optics.*

discussed in section 5.

4 Theoretical methods

The theoretical analysis of magnetooptic rib waveguides as sketched in Fig. 2 is accomplished as follows. First it is assumed that the waveguides are prepared in an isotropic dielectric material and their electromagnetic modal fields are calculated, using different methods. Then the magnetooptic properties are introduced by perturbation theory. They lead to nonreciprocal mode conversion and nonreciprocal phase shifts. Finally these effects are used to design nonreciprocal devices as isolators and circulators.

4.1 Calculation of modal field profiles

It is assumed that the waveguide is homogeneous in z–direction, the direction of light propagation, and that the materials are isotropic and lossless. Thus, the propagating modes are described by their electric and magnetic fields, respectively:

$$\left.\begin{array}{l}\mathbf{E}(x,y)\\ \mathbf{H}(x,y)\end{array}\right\}\exp[i\,(\beta\,z-\omega\,t)]\,, \tag{3}$$

where $\mathbf{E}$ and $\mathbf{H}$ are the components of the mode profile, β denotes the propagation constant, $\omega = c\,k_0$ the frequency and $k_0 = 2\,\pi/\lambda$ the vacuum wavenumber with λ the vacuum wavelength. Maxwell's equations yield for the transverse components of the electric and magnetic field vectors the differential equations:

$$\begin{bmatrix} k_0^2\epsilon + \partial_x \frac{1}{\epsilon}\partial_x\epsilon + \partial_y^2 & \partial_x \frac{1}{\epsilon}\partial_y\epsilon - \partial_x\partial_y \\ \partial_y \frac{1}{\epsilon}\partial_x\epsilon - \partial_y\partial_x & k_0^2\epsilon + \partial_x^2 + \partial_y \frac{1}{\epsilon}\partial_y\epsilon \end{bmatrix} \begin{bmatrix} E_x \\ E_y \end{bmatrix} = \beta^2 \begin{bmatrix} E_x \\ E_y \end{bmatrix}, \tag{4}$$

$$\begin{bmatrix} k_0^2\epsilon + \partial_x^2 + \epsilon\partial_y \frac{1}{\epsilon}\partial_y & \partial_x\partial_y - \epsilon\partial_y \frac{1}{\epsilon}\partial_x \\ \partial_y\partial_x - \epsilon\partial_x \frac{1}{\epsilon}\partial_y & k_0^2\epsilon + \epsilon\partial_x \frac{1}{\epsilon}\partial_x + \partial_y^2 \end{bmatrix} \begin{bmatrix} H_x \\ H_y \end{bmatrix} = \beta^2 \begin{bmatrix} H_x \\ H_y \end{bmatrix}. \tag{5}$$

The longitudinal z–components are determined by the divergence–equations

$$\mathrm{div}\,(\epsilon\,\mathbf{E}) = 0 \qquad \text{and} \qquad \mathrm{div}\,(\mu\,\mathbf{H}) = 0\,. \tag{6}$$

$\epsilon = n_0^2$ denotes the permittivity, where n_0 is the isotropic refractive index, and μ is the permeability of the material. At optical frequencies $\mu = 1$ is a very good approximation.

The equations (4) and (5) are equivalent. They describe the full vectorial modal fields **E** and **H**. However, usually one field component is dominant. If the minor component is neglected, one arrives at the simpler semi–vectorial equations for the quasi TE and quasi TM modes[15, 16]:

$$\textbf{quasi TE:} \qquad \mathbf{E} = \begin{bmatrix} 0 \\ E_y \\ E_z \end{bmatrix} \quad \text{and} \quad \mathbf{H} = \begin{bmatrix} H_x \\ H_y \\ H_z \end{bmatrix} \tag{7}$$

with the wave equation

$$\left[k_0^2\,\epsilon + \partial_x^2 + \partial_y\,\frac{1}{\epsilon}\,\partial_y\,\epsilon\right]\,E_y = \beta_{TE}^2\,E_y \tag{8}$$

and

$$\textbf{quasi TM:} \qquad \mathbf{E} = \begin{bmatrix} E_x \\ E_y \\ E_z \end{bmatrix} \quad \text{and} \quad \mathbf{H} = \begin{bmatrix} 0 \\ H_y \\ H_z \end{bmatrix} \tag{9}$$

with the wave equation

$$\left(k_0^2\,\epsilon + \epsilon\,\partial_x\,\frac{1}{\epsilon}\,\partial_x + \partial_y^2\right)\,H_y = \beta_{TM}^2\,H_y\,. \tag{10}$$

For planar waveguides the partial derivatives with respect to y vanish yielding equations which can be solved analytically.

Numerous methods have been developed to solve the partial differential equations (4,5) or (8,10). Analytical approximations can be applied to obtain a quick

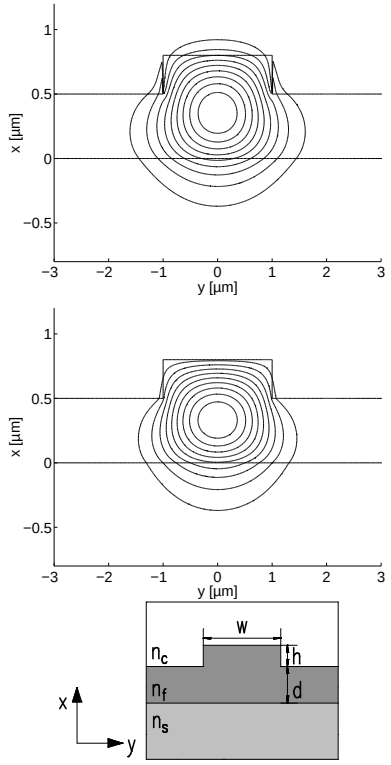

Figure 3: *Contour plots of the main field components $|E_y|$ (top) and $|H_y|$ (center) of the fundamental TE_0 and TM_0 modes, respectively. The contour levels are spaced at 10% of the maximum amplitude. The waveguide parameters (bottom) are: $d = 0.5$ μm, $h = 0.3$ μm, $w = 2.0$ μm, $\lambda = 1.3$ μm and the respective refractive indices are $n_s = 1.9$, $n_f = 2.2$, $n_c = 1.0$.*

overview[17, 18]. More rigorous techniques apply finite element (FEM), finite difference (FDM), rigorous planar eigenmode expansion (film mode matching, FMM) or beam propagation (BPM) methods, however, at the expense of computational effort[19, 15, 16, 20, 21, 22, 23].

A versatile and efficient technique is the wave matching method (WMM)[24, 25]. It is based on a transverse resonance technique. For each region of constant permittivity the modal fields are assumed to be a linear combination of plausible trial solutions which satisfy the differential equations. Interface conditions then yield propagation constants and modal fields.

As an example, Fig. 3 shows the profiles of the TE_0 and TM_0 mode of a typical rib waveguide. These profiles are calculated using the FEM method and the semivectorial approximation. The parameters are listed in the figure caption. Note the discontinuity of the electric field at the vertical boundaries.

4.2 Magnetooptical effects

The magnetooptical properties are described by the nondiagonal components of the permittivity tensor:

$$\hat{\epsilon} = n_0^2 \begin{bmatrix} 1 & 0 & 0 \\ 0 & 1 & 0 \\ 0 & 0 & 1 \end{bmatrix} + K \begin{bmatrix} 0 & M_z & -M_y \\ -M_z & 0 & M_x \\ M_y & -M_x & 0 \end{bmatrix} = n_0^2 \begin{bmatrix} 1 & 0 & 0 \\ 0 & 1 & 0 \\ 0 & 0 & 1 \end{bmatrix} + \Delta\hat{\epsilon}\,. \quad (11)$$

M_j, j=x,y,z, denotes the components of the magnetization. K is a complex material parameter $K = K' + i\,K''$, where K'' is connected to the specific Faraday rotation by:

$$\Theta_{F,sat} = -\,k_0\,\frac{K''\,M_s}{2\,n_0}\,. \quad (12)$$

The real part K' determines the Faraday ellipticity which is neglected in this article. Furthermore, also the Cotton–Mouton effect is omitted, which depends quadratically on the magnetization components and is thus a reciprocal effect.

4.2.1 Nonreciprocal phase shift

The elements of the gyrotropic part $\Delta\hat{\epsilon}$ of the permittivity tensor are small compared to n_0^2 and can thus be treated by perturbation theory[26]. The component M_z, which is parallel to the waveguide axis, gives rise to TE–TM mode coupling and thus to mode conversion, **which is similar to Faraday rotation in bulk media**; it will be treated in section 4.2.3. The components M_x and M_y, which are perpendicular to that axis, induce a change $\delta\beta$ of the propagation constant β, which depends on the propagation direction, $forward$ or $backward$:

$$\beta^{forward} = \beta + \delta\beta \qquad \text{and} \qquad \beta^{backward} = \beta - \delta\beta\,, \quad (13)$$

resulting in a difference $\Delta\beta = 2\,\delta\beta$ between forward and backward propagation constants; β denotes the unperturbed propagation constant. **This nonreciprocal phase shift does not exist in the case of light propagation in bulk materials, because the effect can be viewed as being immediately related to material discontinuities. A simple plausibel explanation can be given using the rough zigzag model of mode propagation in dielectric waveguides. Each reflection at the waveguide boundaries induces a phase shift which depends on the polarization, TE or TM. Furthermore, it depends on the magnetooptical properties of the waveguide structure and this phase shift is nonreciprocal.**

Perturbation theory yields for $\delta\beta$:

$$\delta\beta = \frac{\omega\,\epsilon_0}{N} \int\int \mathbf{E}^*\,\Delta\hat{\epsilon}\,\mathbf{E}\,dx\,dy \tag{14}$$

normalized by the power flow in z–direction

$$N = \left[\int\int \mathbf{E}\times\mathbf{H}^* + \mathbf{E}^*\times\mathbf{H}\right]_z dx\,dy\,. \tag{15}$$

In addition, the components M_x and M_y also cause TE–TM mode coupling which, however, is usually small compared to the coupling by M_z.

Using the semivectorial approximation, equ. (14) can be simplified for quasi TM and quasi TE modes. If $\mathbf{M}$ is parallel to the x–axis, a nonreciprocal phase shift for the TE mode occurs as:

$$\Delta\beta^{TE} = \frac{2\,\omega\,\epsilon_0}{\beta^{TE}\,N} \int\int (K''M_x)\,E_y\,\partial_y\,E_y\,dx\,dy \tag{16}$$

and if $\mathbf{M}$ is parallel to the y–axis the nonreciprocal phase shift for the TM mode is, neglecting second order derivatives with respect to x:

$$\Delta\beta^{TM} = -\frac{2\,\beta^{TM}}{\omega\,\epsilon_0\,N} \int\int \frac{(K''M_y)}{n_0^4}\,H_y\,\partial_x\,H_y\,dx\,dy\,. \tag{17}$$

It is assumed that the waveguide cross section can be divided into rectangles within which material parameters are constant. In this case the double integrals can be converted into a sum of single integrals along the boundaries at which discontinuities of parameters occur:

$$\Delta\beta^{TE} = \frac{2\,\omega\,\epsilon_0}{\beta^{TE}\,N} \sum_m \left(\int (K''M_x)\,|E_y^2|\,dx\,\Big|_{m,v-0} - \int (K''M_x)\,|E_y^2|\,dx\,\Big|_{m,v+0} \right) \tag{18}$$

and

$$\Delta\beta^{TM} = \frac{2\,\beta^{TM}}{\omega\,\epsilon_0\,N} \sum_m \left(\int \frac{(K''M_y)}{n_0^4}\,|H_y^2|\,dy\,\Big|_{m,h-0} - \int \frac{(K''M_y)}{n_0^4}\,|H_y^2|\,dy\,\Big|_{m,h+0} \right). \tag{19}$$

The index m counts the vertical (v) and horizontal (h) lines of discontinuity in x– and y–directions, respectively. $+0$ and -0 indicate that the integrals have to be taken at infinitesimal distances from the lines of discontinuity. To achieve a large nonreciprocal phase shift according to eqns. (18) and (19), it is essential to create a strong discontinuity of the Faraday rotation at the maximum of the mode intensities

or to position such a discontinuity at the mode intensity maximum, respectively. **Eqns. (18,19) show that the magnitude and sign of the nonreciprocal phase shifts $\Delta\beta^{TE,TM}$ depend on the magnitude and sign of the Faraday rotation and on the geometry of the waveguide.**

The TM mode phase shift was first introduced by Yamamoto et al.[27]. The nonreciprocal phase shift of the TE mode was first predicted by Popkov et al.[28], using a rib waveguide parallel to stripe domains. Bahlmann et al.[20] calculated the nonreciprocal phase shift of a TE mode in a rib waveguide with a compensation wall at the rib center parallel to the waveguide using FEM.

As an example Fig. 4 shows the calculated nonreciprocal phase shift of the TM_0 mode for a double and a single layer. For the double layer the maximum of $|\Delta\beta|$ is about 2.5 times larger than for the single layer. In addition, it occurs at a larger film thickness and the dependence of $|\Delta\beta|$ on the film thickness is weaker. These properties are important for practical applications.

The experimental verification of the nonreciprocal TM mode phase shift has been presented by Wallenhorst et al. and by Bahlmann et al.[29, 30]. Some results are shown in Fig. 5. The enhancement of $|\Delta\beta|$ is not as large as shown in Fig. 4 because the absolute value of the Faraday rotation of the positive rotating layer is small due to the high substitution level of gallium, necessary to achieve sign reversal of Faraday rotation.

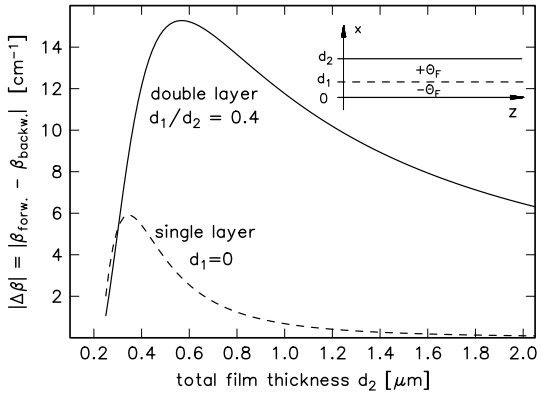

Figure 4: *Calculated nonreciprocal TM_0 mode phase shift $|\Delta\beta|$ for a double and a single layer planar waveguide with a Faraday rotation of 1152°/cm at a wavelength of $\lambda = 1.3\ \mu m$. The refractive indices are $n_c = 1$, $n_f = 2.33$ and $n_s = 1.95$ for the cover region, film and substrate, respectively. The ratio d_1/d_2 is kept fixed at 0.4*[29].

Fehndrich et al.[31] measured the nonreciprocal phase shift of the TE_0 mode of a monomode rib waveguide using a stripe domain lattice parallel to the waveguide having a period equal to the rib width, see Fig. 6. The arrangement with stripe domains perpendicular to the waveguide is used as reference, because this geometry does not induce a nonreciprocal effect. The authors observed a nonreciprocal phase

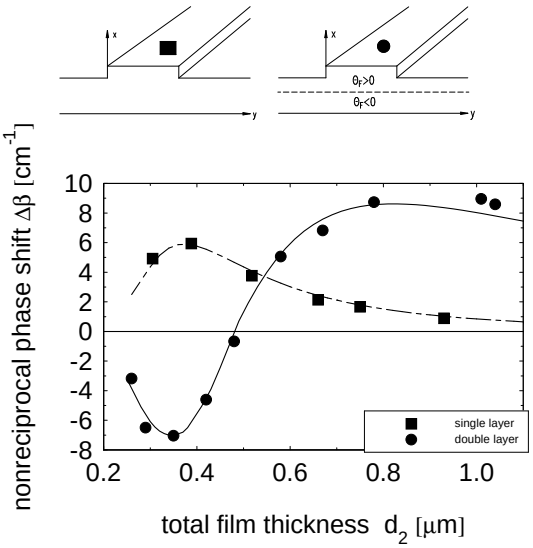

Figure 5: *Calculated and measured nonreciprocal TM_0 mode phase shift for a double and a single layer monomode waveguide versus total film thickness (width 2 μm, height 40 nm)*[30].

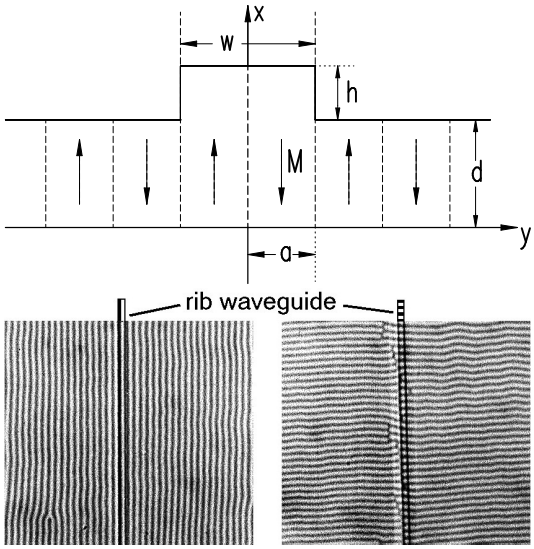

Figure 6: *Principle of the nonreciprocal TE mode phase shift using a stripe domain lattice, top, and experimental arrangement, bottom*[31].

shift of $|\Delta\beta| = (0.8 \pm 0.2)$ cm^{-1}. This value is about half the calculated one. Reasons for the discrepancy are: (i) The domain structure in the 4.9 mm long waveguide may be disturbed, (ii) the cross section of the waveguide may have a trapezoidal rather than a rectangular shape; in this case the mode profile is spatially wider extended causing a decrease of $|\Delta\beta|$.

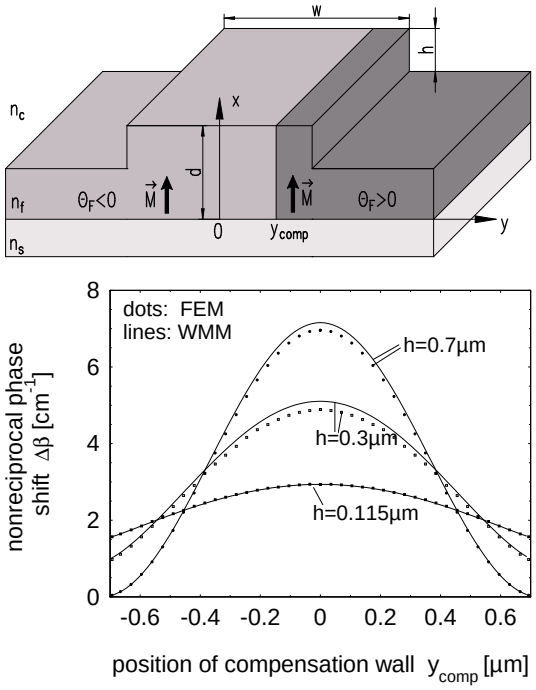

Figure 7: *Top: Principle of the nonreciprocal TE mode phase shift using a compensation wall located inside the rib waveguide. Bottom: Calculated nonreciprocal phase shift as function of the location y_{comp} of the compensation wall. Parameters are: rib width $w = 1.4\,\mu m$, film thickness $d = 0.8\,\mu m$, Faraday rotation $-821°/cm$ at $\lambda = 1.3\,\mu m$; the refractive indices of film, cover and substrate are $n_f = 2.237$, $n_c = 1.0$, $n_s = 1.95$, respectively*[32].

Wilkens et al.[32] used a vertical compensation wall inside a rib waveguide to induce a nonreciprocal phase shift for TE modes. This geometry, shown in Fig. 7, has advantages over the case of a stripe domain lattice, Fig. 6. The compensation wall is fixed and does not change position by applying an external magnetic field. Furthermore, the nonreciprocal phase shift is larger compared to the case of a domain lattice, because all domain walls contribute to $\Delta\beta$ with alternating signs. The authors observed a nonreciprocal phase shift of $|\Delta\beta| = (0.7 \pm 0.2)$ cm^{-1}. According to calculations a $|\Delta\beta|$ of 2.9 cm^{-1} or 1.6 cm^{-1} would be expected if the compensation wall is located at the rib center or at the rib flanks, respectively. Reasons for the discrepancy are: (i) The position of the compensation wall varies along the 5 mm long rib waveguide and is partly outside the rib, (ii) the cross section of the waveguide deviates from rectangular shape. Calculated nonreciprocal phase shifts are presented in Fig. 7, bottom, using FEM and WMM.

Fujita et al.[33] measured a nonreciprocal TE mode phase shift using an asymmetrical waveguide, see section 4.2.2.

For double layer waveguides the layer with positive Faraday rotation is close to the compensation point. Thus, a strong temperature dependence of the nonreciprocal properties arises. This behavior can be improved considerably using a paramagnetic layer and choosing the proper sequence of the different layers as shown in[30, 34].

4.2.2 Waveguides with polarization independent nonreciprocal phase shift

For some of the nonreciprocal integrated devices discussed below it is desirable to use magnetooptical waveguides with a polarization independent nonreciprocal phase shift. To obtain such waveguides discontinuities of the Faraday rotation along horizontal lines as well as along vertical lines are required. A theoretical discussion of such waveguides is presented in[35]. The most promising structure is depicted in Fig. 8. It consists of two layers. The bottom layer is in–plane magnetized, the top layer vertically and the white arrows inicate the direction of the magnetization. The boundary between both layers induces the nonreciprocal TM mode phase shift. The top layer is divided in regions which are oppositely magnetized, parallel or antiparallel to the film normal, the x–axis. In Fig. 8a) there is a periodical change, e. g. a lattice of stripe domains, the lattice period of which equals the rib width. In Fig. 8b) there is only one change at the rib center, e. g. a compensation wall.

The calculated nonreciprocal phase shift is plotted in Fig. 8c) versus the height h_b of the bottom layer. The other parameters are given in the figure caption and by the inset. The WMM is used to obtain the modal fields needed for the perturbation treatment. A nonreciprocal phase shift of $\Delta\beta = 7$ cm^{-1} equal for both, TE and TM modes, is obtained for the case of the compensation wall and of $\Delta\beta = 4$ cm^{-1} for the case of the domain lattice. The smaller value for the stripe domain structure is caused by the fact that the sign of the contribution to the nonreciprocal phase shift alternates at each domain wall.

Fujita et al.[33] proposed an asymmetric waveguide to achieve polarization independent nonreciprocal phase shift. The waveguide consists of a magnetooptical raised strip on a substrate having on one side a paramagnetic or diamagnetic cladding layer of high refractive index. The authors report first experimental results about nonreciprocal phase shift of such a structure.

4.2.3 Nonreciprocal TE–TM mode coupling

If the magnetization is oriented in z–direction along mode propagation, the gyrotropic tensor $\Delta\hat{\epsilon}$ couples the strong x–component of the quasi TE mode to the strong y–component of the quasi TM mode. This coupling leads to periodical power exchange between these modes. Denoting the z–dependent amplitudes of the nor-

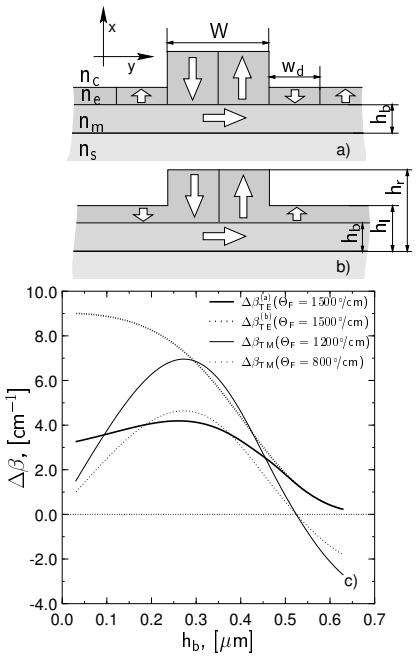

Figure 8: *a,b): Geometries of two different waveguides each consisting of two layers with horizontal and vertical boundaries of discontinuity of the Faraday rotation. c): Calculated nonreciprocal phase shift both for TE and TM modes in the two waveguides versus the thickness h_b of the bottom layer. Waveguide parameters: $n_s = 1.95$, $n_m = 2.2$, $n_e = 2.3$, $n_c = 1.0$, $h_r = 0.7$ μm, $h_l = 0.5$ μm, $W = 1.0$ μm, $w_d = 0.5$ μm, $\lambda = 1.3$ μm*[35].

malized modes by $A^{TE}(z)$ and $A^{TM}(z)$, perturbation theory yields for the variation of the amplitudes along z–direction:

$$\begin{bmatrix} A^{TM}(z) \\ A^{TE}(z) \end{bmatrix} = \exp(\mathrm{i}\,\overline{\beta}\,z) \begin{bmatrix} \cos\Gamma z - \mathrm{i}\frac{\Delta\beta'}{2\Gamma}\sin\Gamma z & -\mathrm{i}\frac{\kappa}{\Gamma}\sin\Gamma z \\ -\mathrm{i}\frac{\kappa^*}{\Gamma}\sin\Gamma z & \cos\Gamma z + \mathrm{i}\frac{\Delta\beta'}{2\Gamma}\sin\Gamma z \end{bmatrix} \begin{bmatrix} A^{TM}(0) \\ A^{TE}(0) \end{bmatrix}, \tag{20}$$

where $\overline{\beta} = (\beta^{TM} + \beta^{TE})/2$, $\Delta\beta' = \beta^{TM} - \beta^{TE}$ and $\Gamma = \sqrt{(\Delta\beta'/2)^2 + |\kappa|^2}$. The coupling constant κ is given by:

$$\kappa = \frac{\omega\,\epsilon_0}{4} \int\int \vec{E}^{*\,TE}\,\Delta\hat{\epsilon}\;\vec{E}^{TM}\,dx\,dy\,. \tag{21}$$

κ is directly proportional to the Faraday rotation and the component of the magnetization parallel to mode propagation.

Assuming that the propagation starts with a purely TE polarized wave, the relative power associated with the TM polarized mode after propagating along the device of

length L is

$$\frac{|A^{TM}(L)|^2}{|A^{TE}(L)|^2} = \frac{|\kappa|^2}{|\kappa|^2 + \Delta\beta^2/4} \sin^2\left(L\sqrt{|\kappa|^2 + \Delta\beta^2/4}\right). \quad (22)$$

It is obvious from equ. (22) that a complete mode conversion can only be achieved for the case of perfect phase matching: $\beta^{TM} = \beta^{TE}$.

5 Nonreciprocal devices

The magnetooptical properties of optical waveguides dicussed above can be used to design nonreciprocal integrated devices like isolators and circulators. Such devices are presented in the following sections.

5.1 Nonreciprocal mode conversion

The first concept of an integrated isolator was based on nonreciprocal TE–TM mode conversion. The nonreciprocal coupling between these modes is caused by the Faraday rotation if the magnetization is aligned along the z–axis, parallel to mode propagation. If the isolator is part of an integrated optical circuit, this concept requires in addition to the 50% nonreciprocal mode conversion another 50% reciprocal conversion, see e. g.[36, 37]. Furthermore, waveguide polarizers are needed.

The main problem of this concept is the phase mismatch between TE and TM modes, $\beta_{TE} \neq \beta_{TM}$. Phase matching has to be adjusted very precisely so that the required isolation can be achieved, see equ. (22). Numerous attempts have been started to solve this problem.

For the particular cases of phase matched rectangular raised strip waveguides and embedded cores with square cross sections, Ref.[38] presents a detailed perturbational description including tolerance analysis of the problem.

Dammann et al.[39] applied stress to the waveguide to control phase matching after fabrication of the isolator. Wolfe et al.[40] used final etch–tuning of the waveguide to get rid of the birefringence between TE and TM modes or they applied a periodic $\Delta\beta = \beta_{TE} - \beta_{TM}$ reversal[41]. In two other attempts an elegant method was developed to adopt the birefringence in the isolator design by choosing an appropriate input polarization[42, 43]; a broadband isolation of more than 30 dB was obtained. Nevertheless, the enormous difficulties to achieve precise phase matching induced the investigation of other isolator concepts.

An interesting nonreciprocal mode conversion is reported by Shintaku[44]. The monomode waveguide he constructed propagates a TM mode in forward direction.

In backward direction, however, the mode experiences a nonreciprocal phase shift and couples now effectively to a radiating TE mode, which is below cut–off. Isolation of 27 dB at $\lambda = 1.535\,\mu$m is achieved.

Another interesting concept is described by Lohmeyer et al.[45]. If in a layered nonreciprocal waveguide with suitable geometry the magnetization is oriented in–plane at intermediate angles, both types of nonreciprocal effects, phase shift and mode conversion, occur simultaneously. By appropriate tuning it should be possible in principle to balance these effects, such that phase matching is realized for one direction of propagation only. The result is a waveguide segment that converts TE to TM polarization (and vice versa) for, say, forward propagation, but keeps the polarization state for light propagating in the backward direction. In Ref.[45] a concept of a four port circulator is discussed, where the described unidirectional polarization converters are combined with polarization splitters.

5.2 Nonreciprocal Mach–Zehnder interferometer

This concept relies on the nonreciprocal phase shift between forward and backward propagating modes. Using this effect, a waveguide Mach–Zehnder interferometer (MZI) can be designed such that in the forward direction the modes in the two arms are in phase yielding constructive interference while in the backward direction the modes are out of phase by 180° causing destructive interference. The first proposal of such a device was presented by Auracher et al.[46].

The principle of a nonreciprocal Mach–Zehnder interferometer is sketched in Fig. 9 for TM modes using rib waveguides. The interferometer arms with nonreciprocal phase shift consist of double layers with opposite sign of Faraday rotation. They are in–plane magnetized perpendicular to mode propagation. In the top interferometer only one arm has nonreciprocal properties. In the bottom interferometer two arms are nonreciprocal. As the magnetization is oppositely directed in the two arms the nonreciprocal phase shift has opposite sign so that the total length of the interferometer is only half of that of the top interferometer. Isolators based on such nonreciprocal Mach–Zehnder interferometers for TM modes are described in[47]. Mach–Zehnder isolators for TE modes are discussed in[48].

An experimental realization of a Mach–Zehnder isolator for TM modes is presented by Fujita et al.[49]. Isolation of 19 dB around 1.553 μm wavelength could be achieved.

5.3 Polarization independent Mach–Zehnder isolators

The waveguides discussed above, having polarization independent nonreciprocal phase shift, can be utilized to realize polarization independent Mach–Zehnder iso-

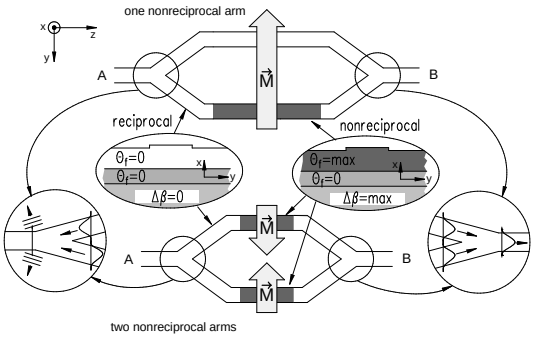

Figure 9: *Principle of a nonreciprocal Mach–Zehnder interferometer for TM modes. Top: One nonreciprocal interferometer arm. Bottom: Two nonreciprocal interferometer arms with opposite sign of the phase shift*[47].

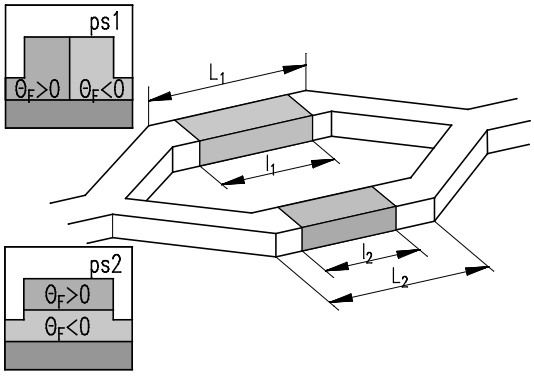

Figure 10: *Principle of a polarization independent MZI–isolator with nonreciprocal TE and TM mode phase shift separated in the two interferometer arms*[50].

lators which are preferable for practical applications.

The first polarization independent Mach–Zehnder isolator is described by Zhuromskyy et al.[50]. The nonreciprocal phase shift is induced for the TE and TM modes separately in the two interferometer arms, see Fig. 10. It turns out that geometric tolerances are very tough.

5.4 Nonreciprocal couplers

A very interesting device is the nonreciprocal X–coupler depicted in Fig. 11. For tight coupling the section of the parallel waveguides can be treated by coupled mode theory. The two fundamental modes are of even and odd symmetry with respect to the centerplane, the x–z–plane, between the parallel waveguides and they have nonreciprocal propagation constants. The coupler can be designed such that the following coupling scheme of the four ports is obtained:

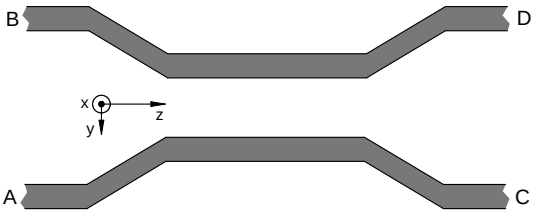

Figure 11: *Principle of a four port nonreciprocal X–coupler*[51].

$$A \Longrightarrow C \Longrightarrow B \Longrightarrow D \Longrightarrow A\,.$$

This coupler acts as a four port circulator and is thus even more versatile than an isolator. The performance of such a nonreciprocal coupler for TM modes is calculated by Bahlmann et al.[51] using FEM and BPM. Fig. 12 presents the calculated parts $A \Longrightarrow C$ and $C \Longrightarrow B$ of the coupling scheme. The discussion of fabrication tolerances shows that post fabrication tuning is necessary.

Another integrated optical circulator based on a coupler geometry is presented by Lohmeyer et al.[52]. It consists of two parallel outer waveguides which are coupled by a third wide, multimode waveguide in between. Conditions for four port circulator performance are discussed.

5.5 Nonreciprocal multimode imaging (MMI)

Nonreciprocal multimode imaging devices have been discussed by Zhuromskyy et al.[53]. They can be applied as isolators and circulators. The basic geometry is sketched in Fig. 13. A section of a multimode waveguide is coupled to two or more monomode input and output waveguides. The input line excites all modes of the MMI section, according to the overlap of mode profiles. These modes give rise to an interference pattern which is periodical along the propagation direction. Thus, after each period an image of the initial light distribution is obtained. At the end of the MMI section the interference pattern causes coupling to the output waveguides. If the waveguides have magnetooptical properties, nonreciprocal effects occur. Fig. 14 shows the intensity distribution for forward and backward propagation of an MMI isolator.

A four port MMI structure is depicted in Fig. 15. It can act as a circulator as sketched in the figure. The calculated performance of such a circulator for TE modes is presented in Fig. 16. Inside the multimode section there is one up and one down domain of equal width located parallel to the waveguide. The vertical lines marked I and II refer to the lengths $L = 3530.5\,\mu$m and $L = 3658.5\,\mu$m of the multimode section, respectively.

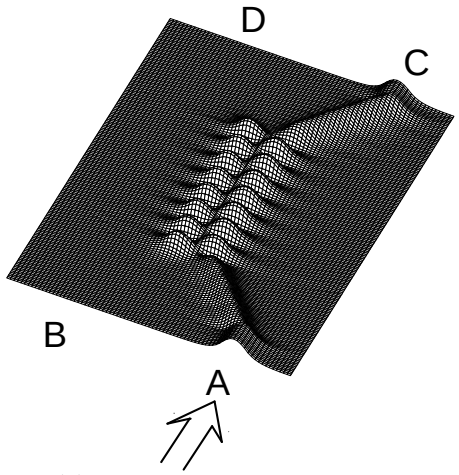

(a) Forward propagation, connection A ⇒ C

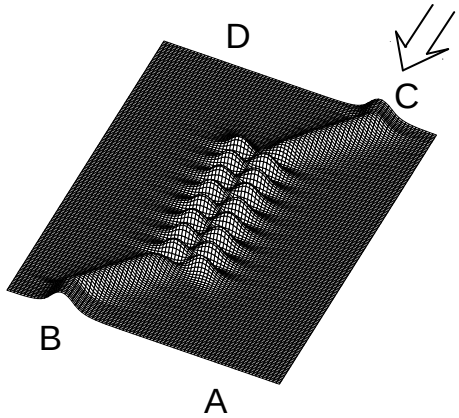

(b) Backward propagation, connection C ⇒ B

Figure 12: *Calculated performance of a four port nonreciprocal X–coupler for TM modes, showing: (a) one of the forward connections (straight, even number of couplings) and (b) one of the backward connections (crossing, odd number of couplings)* [51].

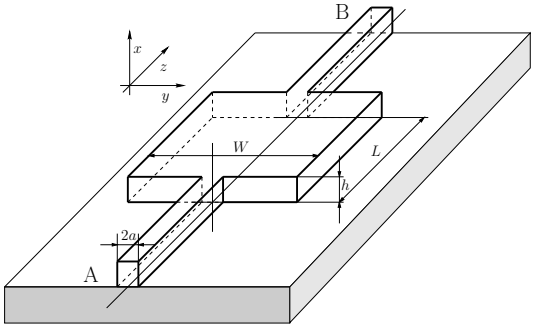

Figure 13: *Principle of a two port MMI structure*[53].

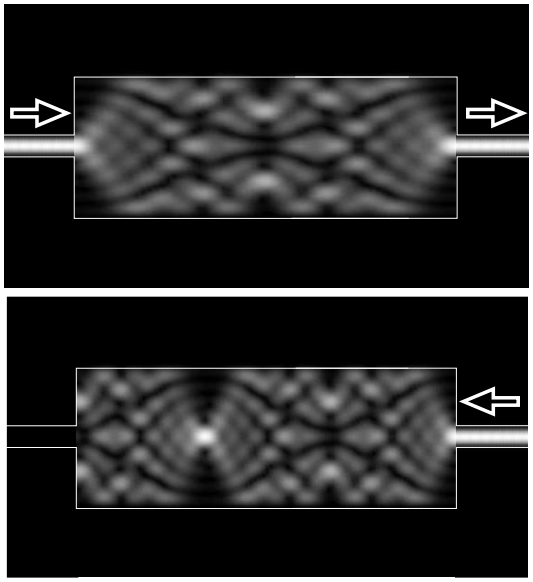

Figure 14: *Calculated intensity distribution of a two port MMI isolator.*

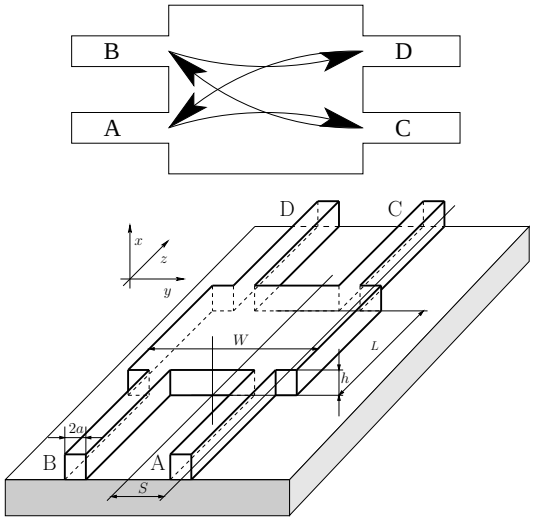

Figure 15: *Principle of a four port MMI structure*[53].

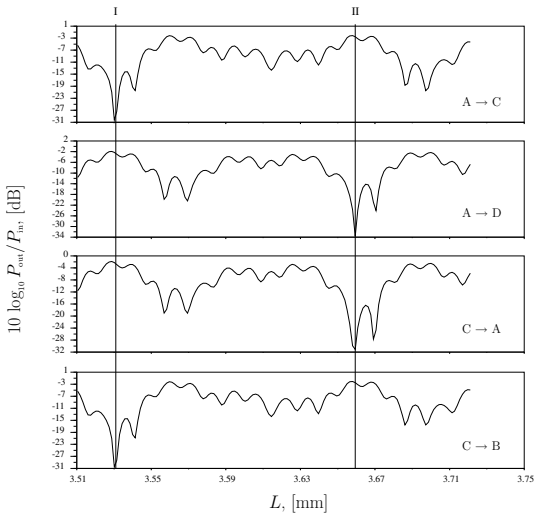

Figure 16: *Calculated performance of a four port nonreciprocal MMI circulator. The ratio between output and input power in dB is plotted versus the length L of the multimode section. The material parameters are* $n_c = 1.0$, $n_f = 2.2$, $n_s = 1.95$, $\Theta_{F,sat} = 2880°/cm$ *and* $\lambda = 1.3\mu m$. *The geometrical parameters, see Fig. 15, are* $h = 0.7\,\mu m$, $a = 0.5\,\mu m$, $W = 4.45\,\mu m$, $S = 1.1\,\mu m$[53].

Cross strip isolator

An interesting variant of nonreciprocal MMI devices is the cross strip isolator, introduced by Lohmeyer et al.[54]. The principle for a TM mode is sketched in Fig. 17. It consists of an in–plane magnetized double layer with opposite sign of Faraday rotation. Light is propagating in z–direction. Perpendicular to this direction a cross strip of variable length $L(y)$ and height h is etched, such that outside this strip the planar waveguide is monomode while in the strip region the vertical fundamental and the first order mode can propagate. The cross strip is of trapezoidal rather than of rectangular shape, however, the angle α is only a few degrees.

The operation of this isolator is as follows: An incoming mode TM_0^{in} excites at the beginning of the cross strip, $z = 0$, the fundamental and first order modes TM_0^L and TM_1^L. Constructive interference of these modes excites at the end of the cross strip, $z = L(y)$, the outgoing mode TM_0^{out}. In backward direction, the interference of the modes is destructive and light is radiated into the cover and mainly into the substrate region. This behavior is simulated in Fig. 18. The calculated performance of such an isolator at a central wavelength of $\lambda = 1.3\,\mu m$ is presented in Fig. 19. It is also shown that reflections at the boundaries of the cross strip can be neglected. The additional and important advantage of this isolator is the possibility to adjust the interference by varying the strip length $L(y)$ by shifting the input coupling along the y–direction. First experimental result of this type of isolator are given in Ref.[55].

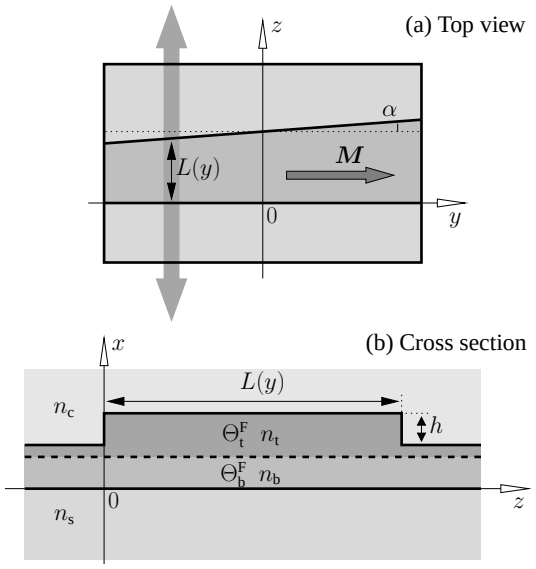

Figure 17: *Principle of a cross strip isolator, showing: (a) top view, (b) cross section*[54].

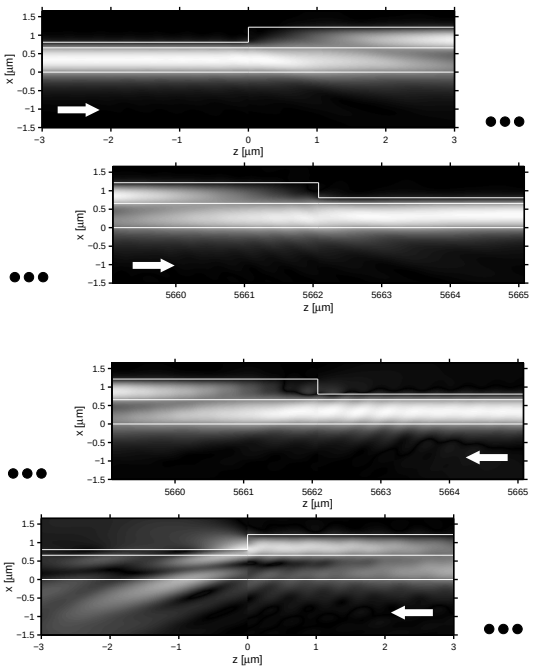

Figure 18: *Simulation of the operation of a cross strip isolator. Top two lines: forward propagation, bottom two lines: backward propagation.*[54].

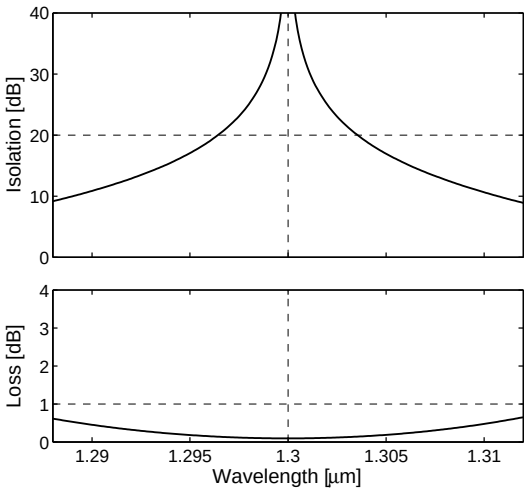

Figure 19: *Calculated performance of a cross strip isolator. Top: isolation, bottom: forward loss*[54].

6 Integration techniques

Even if a waveguide garnet isolator would be available, its integration with a semiconductor laser remains a severe problem which is mainly twofold.

i) It is necessary to combine these different materials into the same device using chemical and/or physical techniques.
ii) The refractive index of garnets is around 2.4, while that of semiconductors is in the range of 3.5. Thus, optical modes are strongly confined to the semiconductor waveguides hindering the penetration of mode fields into the adjacent garnet structures.

Various techniques have been applied to grow semicondutors on garnet substrates[56, 57]. More recently, it was demonstrated that direct wafer bonding is a promising technique to combine magnetic garnets and semiconductor materials[58, 59]. Especially silicon on insulator (SOI) looks as a very interesting platform for integrated optics. Using special design of the interface of the bonded wafers a strong overlap of modal fields between semiconductor and garnet film can be achieved leading to a considerable enhancement of the nonreciprocal phase shift of the TM_0 mode[60, 61].

An interesting hybrid solution for an optical isolator is presented by Sugimoto et al.[62]. The authors obtained an isolation of more than 25 dB at a forward loss below 3.2 dB in the wavelength range around 1.55 μm.

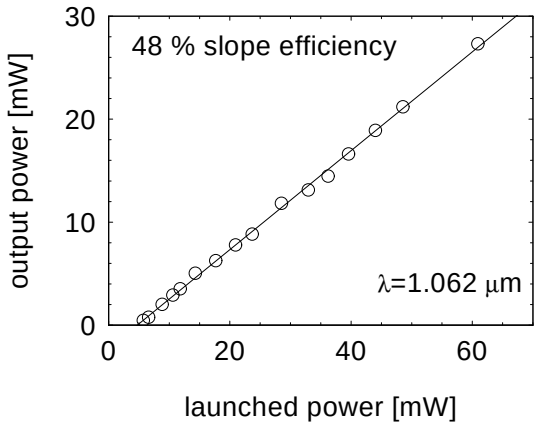

Figure 20: *Differential efficiency of a Nd:GGG channel waveguide laser.*[72].

7 Garnet-waveguide lasers

A further possibility to solve the above mentioned material problems is the fabrication of channel lasers in garnet substrates which can more easily be integrated with garnet–isolators. Although such lasers have to be pumped optically by semiconductor diode lasers, the performance of the latter is not as critical as that of the semiconductor lasers used directly as light sources in optical communication systems.

Among garnet laser crystals, yttrium aluminium garnet (YAG) and gadolinium gallium garnet (GGG) are the most commonly used laser hosts. Especially the GGG substrates are best suited for integration with isolators. Waveguides for laser applications can be prepared by liquid phase epitaxy (LPE), ion implantation[63, 64], pulsed laser deposition (PLD)[65] and thermal bonding[66].

Successful laser operation in planar waveguides of Nd:GGG and of Nd:YAG is reported in Refs.[64, 66, 67, 68, 69]. The highest slope efficiency of 14% is achieved by Chartier et al.[68] for an LPE grown Nd:YAG planar waveguide laser at a threshold of 14 mW.

A monomode channel waveguide Nd:GGG laser is presented by Field et al.[70]. A slope efficiency of 27% and a 8 mW threshold at a wavelength of 1.062 μm are reported. A buried channel waveguide of Yb:GGG is described by Shimokozono et al.[71] achieving a slope efficiency of 14%. Gerhardt et al.[72] fabricated a channel waveguide in Nd:GGG. The performance is presented in Fig. 20. In the meantime the threshold of this laser has been decreased to 5 mW. The laser is pumped at a wavelength of 0.807 μm. The laser is operated without selecting mirrors, thus it lases at the strongest laser wavelength of 1.062 μm.

For practical applications it is desirable to prepare an erbium laser in a garnet

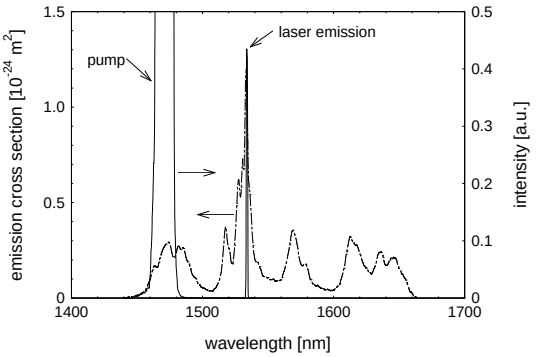

Figure 21: *Laser emission of an Er:GGG channel waveguide laser*[73].

substrate which is lasing at a wavelength around 1.55 μm, which is used for optical communication via glass fiber. Concerning integration with an isolator, the best idea would be to use as host crystal yttrium iron garnet (YIG). However, excited state quenching by Fe^{3+} ions is too strong preventing realization of such a laser. Schröter[73] prepared an channel waveguide laser in Er:GGG. Fig. 21 shows the laser line at $\lambda = 1.534\,\mu$m and the pump line at $\lambda = 1.480\,\mu$m together with the emission spectra. A threshold of 84 mW is observed. However, this threshold can be reduced if a pump at $0.980\,\mu$m is used.

Conclusion

During recent decades integrated nonreciprocal devices for optical communication have been investigated intensively. Activities now concentrate on nonreciprocal phase shift in combination with Mach–Zehnder interferometers rather than on nonreciprocal mode conversion. Considerable progress is achieved towards practical solutions.

Theoretical tools to simulate and modulate optical circuits are developed to a high standard. Numerous concepts have been designed and discussed theoretically, including polarization independent devices.

The experimental techniques to prepare single mode waveguides and to characterize such waveguides are very well established. However, up to now only few of the theoretical models are realized and tested experimentally. The very strict geometrical tolerances form a severe barrier to overcome. The promising devices based on multi–mode–imaging should gain more attention.

The combination of garnets with semiconductor materials has been successfully demonstrated using wafer bonding.

However, despite of the large progress achieved, a lot more effort is needed till practical waveguide versions of nonreciprocal devices integrated with semiconductor lasers will be available. In the meantime, hybrid solutions must be used.

Acknowledgment

Financial support by Deutsche Forschungsgemeinschaft (Sonderforschungsbereich 225 'Oxidische Kristalle für elektro– und magnetooptische Anwendungen') is gratefully acknowledged. For kind permissions to reproduce the following Figures we thank the American Institute of Physics (Fig. 6, Fig. 7, and Fig. 20), Springer (Fig. 13, Fig. 15, and Fig. 16) and IEEE (Fig. 8 and Fig. 10).

REFERENCES

1. A.D. Fisher, J.N. Lee, E.S. Gaynor, and A.B. Tveten, "Optical guided-wave interactions with magnetostatic waves at microwave-frequencies," Appl. Phys. Lett. **41**, 779–781 (1982).

2. H. Tamada, M. Kaneko, and T. Okamoto, "TM–TE optical–mode conversion induced by a transversely propagating magnetostatic wave in a (BiLu)3Fe5O12 film," J. Appl. Phys. **64**, 554–559 (1988).

3. S.H. Talisa, "The collinear interaction between forward volume magnetostatic waves and guided light in YIG films," IEEE Trans. MAG **24**, 2811–2813 (1988).

4. C.S. Tsai and D. Young, "Magnetostatic–forward–volume–wave–based–guided–wave magnetooptic Bragg cells and applications to communications and signal processing," IEEE Trans. MTT **38**, 560–570 (1990).

5. C.S. Tsai and D. Young, "Wideband scanning of a guided–light beam and spectrum analysis using magnetostatic waves in an yttrium iron garnet–gadolinium gallium garnet wave–guide," Appl. Phys. Lett. **54**, 196–198 (1989).

6. B. Neite and H. Dötsch, "Dynamical Conversion of Optical Modes in Garnet Films Induced by Ferrimagnetic Resonance," J. Appl. Phys. **62**, 648–652 (1987).

7. H.P. Winkler, H. Dötsch, B. Lührmann, and S. Sure, "Dynamic conversion of optical modes in magnetic garnet films induced by resonance of periodic stripe domains," J. Appl. Phys. **76**, 3272–3278 (1994).

8. B. Stegmueller, E. Baur, and M. Kicherer, "15–GHz modulation performance of integrated DFB laser diode EA modulator with identical multiple-quantum-well double–stack active layer," IEEE PHOTONIC TECH. Lett. **14**, 1647–1649 (2002).

9. L. Wilkens, D. Träger, H. Dötsch, A. M. Alexeev, A. F. Popkov, and V. I. Korneev:, "Compensation walls in gallium and aluminium substituted gadolinium–bismuth–iron garnet films created by laser annealing: Measurements and simulations," J. Appl. Phys. **93**, 2839–2847 (2003).

10. S.L. Blank and J.W. Nielsen, "The growth of magnetic garnets by liquid phase epitaxy," J. Cryst. Growth **17**, 302–311 (1972).

11. J.P. Krumme, V. Doormann, and B. Strocka, "Selected–area sputter epitaxy of iron–garnet films," J. Appl. Phys. **60**, 2065–2068 (1986).

12. S. Kahl and A.M. Grishin, "Pulsed laser deposition of $Y_3Fe_5O_{12}$ and $Bi_3Fe_5O_{12}$ films on garnet substrates," J. Appl. Phys. **93**, 6945–6947 (2002).

13. P. Hansen, C. P. Klages, J. Schuldt, and K. Witter, "Magnetic and magneto–optical properties of bismuth–substituted lutetium iron garnet films," Phys. Rev. B **31**, 5858–5864 (1985).

14. M. Gomi, K. Satoh, and M. Abe, "Giant Faraday rotation of Ce–substituted YIG films epitaxially grown by RF sputtering," Jap. J. Appl. Phys. **27**, L1536–L1538 (1988).

15. M. S. Stern, "Semivectorial polarized finite difference method for optical waveguides with arbitrary index profiles," IEE Proc. **135**, 56–63 (1988).

16. M. S. Stern, "Semivectorial polarized H field solutions for dielectric waveguides with arbitrary index profiles," IEE Proc. **135**, 333–338 (1988).

17. K.S. Chiang, "Analysis of the effective–index method for the vector modes of rectangular–core dielectric waveguides," IEEE Trans. MTT **44**, 692–700 (1996).

18. P.N. Robson and P.C. Kendall. Rib waveguide theory by the spectral index method. (Wiley, New York, 1990).

19. B.M.A Rahmann and J.B. Davies, "Finite–element solution of integrated optical waveguides," J. Lightw. Techn. **2**, 682–687 (1984).

20. N. Bahlmann, M. Lohmeyer, H. Dötsch, and P. Hertel, "Finite–element analysis of nonreciprocal phase shift for TE modes in magnetooptic rib waveguides with a compensation wall," IEEE Quant. Electr. **35**, 250–253 (1999).

21. F. Wijnands, H.J.W.M Hoekstra, G.J.M Krijnen, and R.M. de Ridder, "Modal fields calculation using the finite difference beam propagation method," J. Lightw. Techn. **12**, 2066–2072 (1994).

22. J. Yamauchi, G. Takahashi, and H. Nakano, "Full–vectorial beam–propagation method based on the McKee–Mitchell scheme with improved finite–difference formulas," J. Lightw. Techn. **16**, 2458–2464 (1998).

23. A.S. Sudbo, "Film mode matching: a versatile numerical method for vector mode field calculations in dielectric waveguides," Pure and Appl. Optics **2**, 211–233 (1993).

24. M. Lohmeyer, "Wave–matching method for mode analysis of dielectric waveguides," Optical and Quantum Electr. **29**, 907–922 (1997).

25. M. Lohmeyer, "Vectorial wave–matching mode analysis of integrated optical waveguides," Optical and Quantum Electr. **30**, 385–396 (1998).

26. G.J. Gabriel and M.E. Brodwin, "The solution of guided waves in inhomogeneous anisotropic media by perturbation and variational methods," IEEE Trans. MTT **13**, 364–370 (1965).

27. S. Yamamoto and T. Makimoto, "Circuit theory for a class of anisotropic and gyrotropic thin–film optical waveguides and design of nonreciprocal devices for integrated optics," J. Appl. Optics **45**, 882–888 (1974).

28. A.F. Popkov, M. Fehndrich, M. Lohmeyer, and H. Dötsch, "Nonreciprocal TE mode phase shift by domain walls in magnetooptic rib waveguides," Appl. Phys. Lett. **72**, 2508–2510 (1998).

29. M. Wallenhorst, M. Niemöller, H. Dötsch, P. Hertel, R. Gerhardt, and B. Gather, "Enhancement of the Nonreciprocal Magnetooptic Effect of TM Modes Using Iron Garnet Double Layers with Opposite Faraday Rotation," J. Appl. Phys., **77**, 2902–2905 (1995).

30. N. Bahlmann, V. Chandrasekhara, A. Erdmann, R. Gerhardt, P. Hertel, R. Lehmann, D. Salz, F.J. Schröteler, M. Wallenhorst, and H. Dötsch, "Improved design of magnetooptic rib waveguides for optical isolators," J. Lightw. Techn. **16**, 818–823 (1998).

31. M. Fehndrich, A. Josef, L. Wilkens, J. Kleine–Börger, N. Bahlmann, M. Lohmeyer, P. Hertel, and H. Dötsch, "Experimental investigation of the nonreciprocal phase shift of a transverse electric mode in a magneto–optic rib waveguide," Appl. Phys. Lett., **74**, 2918–2920 (1999).

32. L. Wilkens, D. Träger, A.F. Popkov, A. Alexeev, and H. Dötsch, "Nonreciprocal phase shift of TE modes induced by a compensation wall in a magneto-optic rib waveguide," Appl. Phys. Lett., **79**, 4292–4294 (2001).

33. J. Fujita, M. Levy, R.M. Osgood, Jr., L. Wilkens, and H. Dötsch, "Polarization–indpendent waveguide optical isolator based on nonreciprocal phase shift," IEEE Photonics Techn. Lett. **12**, 1510–1512 (2000).

34. N. Bahlmann, M. Wallenhorst, L. Wilkens, V. Backherms, A. Josef, P. Hertel, and H. Dötsch, "Reduction of the temperature dependence of the nonreciprocal effect of magnetooptic channel waveguides," Appl. Optics **38**, 5747–5751 (1999).

35. O. Zhuromskyy, H. Dötsch, M. Lohmeyer, L. Wilkens, and P. Hertel, "Magnetooptical waveguides with polarization–independent nonreciprocal phase shift," J. Lightw. Techn. **19**, 214–221 (2001).

36. K. Ando, T. Okoshi, and N. Koshizuka, "Waveguide magnetooptic isolator fabricated by laser annealing," Appl. Phys. Lett. **53**, 4–6 (1988).

37. T. Mizumoto, Y. Kawaoka, and Y. Naito, "Waveguide–type optical isolator using the Faraday and Cotton–Mouton effects," Trans. IECE Jap. **E69**, 968–972 (1986).

38. M. Lohmeyer, N. Bahlmann, O. Zhuromskyy, H. Dötsch, and P. Hertel, "Phase matched rectangular magnetooptic waveguides for applications in integrated optical isolators: numerical assessment," Opt. Comm. **158**, 189–200 (1998).

39. H. Dammann, E. Pross, and G. Rabe, "Phase matching in symmetrical single–mode magnetooptic waveguides by application of stress," Appl. Phys. Lett. **49**, 1755–1757 (1986).

40. R. Wolfe, V.J. Fratello, and M. NcGlashan-Powell, "Elimination of birefringence in garnet–films for magnetooptic wave–guide devices," Apl. Phys. Lett. **51**, 1221–1223 (1987).

41. R. Wolfe, J. Hegarty, J.F. Dillon, Jr., L.C. Luther, G.K. Celler, L.E. Trimble, and C.S. Dorsey, "Thin–film waveguide magnetooptic isolator," Appl. Phys. Lett. **46**, 817–819 (1985).

42. H. Dammann, E. Pross, G. Rabe, and W. Tolksdorf, "45° waveguide isolators with phase mismatch," Appl. Phys. Lett. **56**, 1302–1304 (1990).

43. R. Wolfe, J.F. Dillon, Jr., R.A. Liebermann, and V.J. Fratello, "Broadband magnetooptic waveguide isolator," Appl. Phys. Lett. **57**, 960–962 (1990).

44. T. Shintaku, "Integrated optical isolator based on efficient nonreciprocal radiation mode conversion," Appl. Phys. Lett. **73**, 1946–1948 (1998).

45. M. Lohmeyer, N. Bahlmann, O. Zhuromskyy, H. Dötsch, and P. Hertel, "Unidirectional magnetooptic polarization converters," J. Lightw. Techn. **17**, 2605–2611 (1999).

46. F. Auracher and H.H. Witte, "A new design for an integrated optical isolator," Opt. Comm. **13**, 435–438 (1975).

47. N. Bahlmann, M. Lohmeyer, M. Wallenhorst, H. Dötsch, and P. Hertel, "A comparison of an improved design for two integrated optical isolators based on nonreciprocal Mach–Zehnder interferometry," in Symposium Proceedings on High–density magnetic recording and integrated magnetooptics: Materials and devices **517**, J. Bain, M. Levy, J. Lorenzo, T. Nolan, Y. Okamura, K. Rubin, B. Stadler, R. Wolfe, ed. (Materials Research Society, Warrendale, Pennsylvania, USA, 1998), p. 513–518.

48. N. Bahlmann, M. Lohmeyer, H. Dötsch, and P. Hertel, "Integrated magnetooptic Mach–Zehnder isolator for TE modes," Electr. Lett. **34**, 2122–2123 (1998).

49. J. Fujita, M. Levy, R.M. Osgood, Jr., L. Wilkens, and H. Dötsch, "Waveguide optical isolator based on Mach-Zehnder interferometer," Appl. Phys. Lett., **76**, 2158–2160 (2000).

50. O. Zhuromskyy, M. Lohmeyer, N. Bahlmann, H. Dötsch, P. Hertel, and A.F. Popkov, "Analysis of polarization independent Mach–Zehnder–type integrated optical isolator," J. Lightw. Techn. **17**, 1200–1205 (1999).

51. N. Bahlmann, M. Lohmeyer, O. Zhuromskyy, H. Dötsch, and P. Hertel, "Nonreciprocal coupled waveguides for integrated optical islators and circulators for TM modes," Optics Comm. **161**, 330–337 (1999).

52. M. Lohmeyer, M. Shamonin, N. Bahlmann, P. Hertel, and H. Dötsch, "Radiatively coupled waveguide concept for an integrated magnetooptic circulator," in Symposium Proceedings on High–density magnetic recording and integrated magnetooptics: Materials and devices **517**, J. Bain, M. Levy, J. Lorenzo, T. Nolan, Y. Okamura, K. Rubin, B. Stadler, R. Wolfe, ed. (Materials Research Society, Warrendale, Pennsylvania, USA, 1998), p. 519–524.

53. O. Zhuromskyy, M. Lohmeyer, N. Bahlmann, P. Hertel, H. Dötsch, and A.F. Popkov, "Analysis of nonreciprocal light propagation in multimode imaging devices," Opt. Quant. Electr. **32**, 885–897 (2000).

54. M. Lohmeyer, L. Wilkens, O. Zhuromskyy, H. Dötsch, and P. Hertel, "Integrated magnetooptic cross strip isolator," Optics Comm. **189**, 251–259 (2001).

55. L. Wilkens, "Optimierung und Realisierung integriert–optischer Isolatorkonzepte," PhD Thesis, University of Osnabrück, Germany (2002) (in German).

56. J. Haisma, A.M.W. Cox, B.H. Koek, D. Mateika, J.A. Pistorius, and E.T.J.M. Smeets, "Heteroepitaxial growth of InP on garnet," J. Cryst. Growth **87**, 180–184 (1987).

57. M. Razeghi, P.L. Meunier, and P. Maurel, "Growth of GaInAs–InP multiquantum wells on garnet (GGG=$Gd_3Ga_5O_{12}$) substrate by metalorganic chemical vapor deposition," Appl. Phys. Lett. **59**, 2261–2263 (1986).

58. H. Yokoi, T. Mizumoto, K. Maru, and Y. Naito, "Direct bonding between InP and rare–earth iron–garnet grown on $Gd_3Ga_5O_{12}$ substrate by liquid–phase epitaxy," Electr. Lett. **31**, 1612–1613 (1995).

59. T. Izuhara, J. Fujita, and M. Levy, "Integration of magnetooptical waveguides onto a III–V semiconductor surface," IEEE Photonic Techn. L. **14**, 167–169 (2002).

60. H. Yokoi, T. Mizumoto, and Y. Shoji, "Optical nonreciprocal devices with a silicon guiding layer fabricated by wafer bonding," Appl. Optics **42**, 6605–6612 (2003).

61. R.L. Espinola, T. Izuhara, Ming–Chun Tsai, R.M. Osgood, Jr., and H. Dötsch, "Magnetooptical nonreciprocal phase shift in garnet/silicon–on–insulator waveguides," Opt. Lett. **29**, 941–943 (2004).

62. N. Sugimoto, H. Terui, A. Tate, Y. Katoh, Y. Yamada, A. Sugita, A. Shibukawa, and Y. Inoue, "A hybrid integrated waveguide isolator on a silica–based planar lightwave circuit," J. Lightw. Techn. **14**, 2537–2546 (1996).

63. L. Zhang, P. J. Chandler, P. D. Townsend, S. J. Field, D. C. Hanna, D. P. Shepherd, and A. C. Tropper, "Characterization of ion–implanted wave–guides in Nd–YAG," J. Appl. Phys. **69**, 3440–3446 (1991).

64. S. J. Field, D. C. Hanna, A. C. Large, D. P. Shepherd, A. C. Tropper, P. J. Chandler, P. D. Townsend, and L. Zhang, "An efficient, diode–pumped, ion–implanted Nd–GGG planar wave–guide laser," Opt. Comm. **86**, 161–166 (1991).

65. A. A. Anderson, C. L. Bonner, D. P. Shepherd, R. W. Eason, C. Grivas, D. S. Gill, and N. Vainos, "Low loss (0.5 dB/cm) Nd:Gd3Ga5O12 waveguide layers grown by pulsed laser deposition," Opt. Comm. **144**, 183–186 (1997).

66. C. T. A. Brown, C. L. Bonner, T. J. Warburton, D. P. Shepherd, A. C. Tropper, and D. C. Hanna, "Thermally bonded planar waveguide lasers," Appl. Phys. Lett. **71**, 1139–1141 (1997).

67. S. J. Field, D. C. Hanna, D. P. Shepherd, A. C. Tropper, P. J. Chandler, P. D. Townsend, and L. Zhang, "Ion–implanted Nd–YAG wave–guide lasers," IEEE J. QE **27**, 428–433 (1991).

68. I. Chartier, B. Ferrand, D. Pelenc, S. J. Field, D. C. Hanna, A. C. Large, D. P. Shepherd, and A. C. Tropper, "Growth and low–threshold laser oscillation of an epitaxially grown Nd YAG wave–guide," Opt. Lett. **17**, 810–812 (1992).

69. C. L. Bonner, A. A. Anderson, R. W. Eason, D. P. Shepherd, D. S. Gill, C. Grivas, and N. Vainos, "Performance of a low–loss pulsed–laser deposited Nd:Gd3Ga5O12 waveguide laser at 1.06 and 0.94 μm," Opt. Lett. **22**, 988–990 (1997).

70. S. J. Field, D. C. Hanna, A. C. Large, D. P. Shepherd, A. C. Tropper, P. J. Chandler, P. D. Townsend, and L. Zhang, "Ion–implanted Nd–GGG channel wave–guide laser," Opt. Lett. **17**, 52–54 (1992).

71. M. Shimokozono, N. Sugimoto, A. Tate, and Y. Katoh, "Room–temperature operation of an Yb–doped Gd3Ga5O12 buried channel waveguide laser at 1.025 μm wavelength," Appl. Phys. Lett. **68**, 2177–2179 (1996).

72. R. Gerhardt, J. Kleine-Börger, L. Beilschmidt, M. Frommeier, B. Gather, and H. Dötsch, "Efficient channel–waveguide laser in Nd:GGG at 1.062 mm wavelength," Appl. Phys. Lett. **75**, 1210–1212 (1999).

73. J. Schröter, "Wellenleiterlaser in erbiumdotierten epitaktischen Granatfilmen," PhD Thesis, University of Osnabrück, Germany (2002) (in German).